PERTANIKA
JOURNALS

Full-Scaled Impulse Turbine Performance Prediction using Numerical Simulation

A. Sahed* and F. B. Ismail Alnaimi

Mechanical Department, Curtin University, Sarawak Campus CDT 250, 98009 Miri, Sarawak, Malaysia

ABSTRACT

This paper presents the numerical modelling techniques for the simulation of the energy conversion chain from wave to electricity in an Oscillating Water Column (OWC) equipped with a full-scaled self rectifying turbine. The performance of the OWC device has been assessed for the stand-alone power system of a typical Irish climatic wave condition. The results showed that the overall performance of the complete device depends on the level of turbine damping, which in turn depends on the wave climate, especially the significant wave height. Furthermore, turbine efficiency predicted using quasi-steady showed qualitatively favourable agreement with the experimental results.

Keywords: Wave energy, applied damping, numerical simulation, irregular, unsteady, real sea conditions

INTRODUCTION

The OWC device wave energy harnessing method is considered as one of the best techniques for converting wave energy into electricity. It is an economically viable design due to its simple geometrical construction, and it is also strong enough to withstand against the waves with different heights, periods and directions. The design (see Fig.1) consists of an OWC chamber and a circular duct, which reciprocally move the air from and into the chamber as the wave enters and intercedes from the chamber. The wave energy is converted into air pneumatic energy inside the chamber. A self rectifying impulse turbine mounted inside the duct was designed to turn in one direction only although the airflow moves bi-directionally. This converts the air pneumatic energy to a mechanical power. A matching generator is coupled to the turbine to produce electricity (de O. Falca~o, 2003).

The performance prediction of the impulse turbine under real sea conditions is very important for designers to get a feel for the behaviour of the power converting device under unsteady, irregular flow conditions. This present study deals with the performance

E-mail addresses:
amazighihi@gmail.com (A. Sahed),
fbalnaimi@curtin.edu.my (F. B. Ismail Alnaimi)
*Corresponding Author

prediction of 1.6m diameter impulse turbine with fixed guide vanes under these conditions using numerical simulation. The small scale (0.6m diameter) turbine performance has already been investigated by a few authors (Thakker *et al.,* 2001, 2004) and the numerical simulation technique has also been validated.

The numerical simulation procedure used in this analysis is similar to that used in [3] who investigated the performance of a small scale turbine for various fixed speeds during a time frame of around 260s operating condition. As a next step, the full-scaled turbine performance was analyzed numerically under simulated irregular and unsteady conditions based on real sea data, taking into account the effects due to applied damping provided by the turbine for a period of a year. The effect of the turbine rotational speed on the device efficiency was investigated. The turbine power output was also investigated for various rotational speeds.

Apart from the obvious function of quantifying the performance of turbines and providing a basis for comparing performance, experimental data and the associated dimensional analysis allow the designer to size a turbine to a given wave power application. In contrast to the general design problem familiar in the industry, where a turbine is expected to operate at a single design point for the majority of the time, designing a turbine to a wave power application requires that a design range be taken into account, rather than a single design point (Thakker & Fergal, 2004).
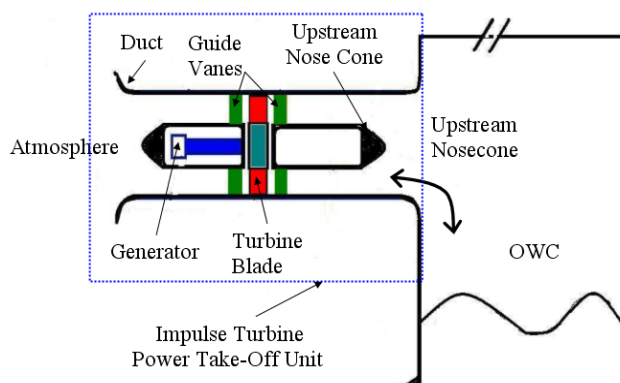
Fig.1: Impulse turbine power take-off with OWC

EXPERIMENTAL AND BACKGROUND

Turbine Design and Manufacture

The basic turbine design parameters were based on the optimum design parameters given by Setoguchi *et al.* [5], but with an H/T ratio of 0.6 [6]. The details, for both 0.6*m* and 1.6*m*, are given in Table 1 and a 2D sketch at the mid radius is shown in Figure 2. The turbine consists of 30 blades and 26 fixed angle mirror image guide vanes on both sides of the rotor. The guide vanes inlet/outlet angle is fixed at 30°. The next step is the design analysis of the next generation impulse turbine for which a preliminary diameter of 1.6*m* was established, and G.F.R.P was selected as the optimum material to manufacture the blades (Thakker *et al.*, 2008).

Experimental Analysis

The overall performance of the turbines was evaluated by the turbine angular velocity, ω, torque generated, T, flow rate, Q, and total pressure drop, ΔP across the rotor. The results were expressed in the forms of torque coefficient, C_T, input power coefficient, C_A and efficiency, η in terms of flow coefficient, φ, which are defined by Setogushi *et al.,* 2006. and the test Reynolds number based on the chord was 0.4×10^4.

$$C_T = \frac{T}{\frac{1}{2}\rho a(\upsilon a^2 + U_R^2)bZL_r r_R} \tag{1}$$

$$C_A = \frac{\Delta PQ}{\frac{1}{2}\rho a(\upsilon a^2 + U_R^2)bZL_r \upsilon_a} \tag{2}$$

$$\phi = \frac{\upsilon_a}{U_R} \tag{3}$$

$$R_e = \frac{\rho a \sqrt{\upsilon a^2 + U_R^2} L_r}{\mu} \tag{4}$$

$$\eta = \frac{C_T}{C_A \phi} \tag{5}$$

The 0.6*m* turbine was tested for different constant axial velocities between a rotational speed range of 1200*rpm* and 100*rpm*, thus, giving a flow coefficient range between 0.15 and 3.58 (Ryan, 2005). The lowest Reynolds number achieved at peak efficiency was 0.46×10^5 at the axial velocity of 4.91*m=s* and the highest *Re* was 1.23 105 at $v_a = 12.6 m/s$, respectively. These upper and lower limits were defined by the limitations of the test rig; the experiments were carried out up to a flow rate of 2.11*m³*/s and the instruments used for data collection. It is believed that there are no prominent effects of Reynolds number on this type of turbine and constant performance can be achieved over a wide range of Reynolds number (0.46×10^5 to 1.23×10^5), as the mean efficiency is within ±2.5% of the maximum and the minimum efficiencies achieved within this range of Reynolds number. Furthermore, the critical Reynolds number found experimentally for this turbine was 0.65×10^5 (Ryan, 2005; Hammad, n.d). In general, it can be said that this type of impulse turbine has no apparent effects due to the change in the Reynolds number as the performance was found to be stable over a wide range of Re.

TABLE 1
Rotor and guide vane parameters

Parameter	Symbol	0.6∅	1.6∅
Blade profile: elliptical			
Hub-to-tip ratio	HT	0.6	0.6
Number of blades	z	30	30
Chord length (mm)	l_r	100	268
Pitch (mm)	S_r	50	134
Blade inlet angle	γ	60°	60°
Guide vanes profile: plate type			
Pitch (mm)	S_g	58	154
Chord length (mm)	l_g	131	352
Number of guide vanes	g	26	26
Guide vane inlet/outlet angle	γ	30°	30°
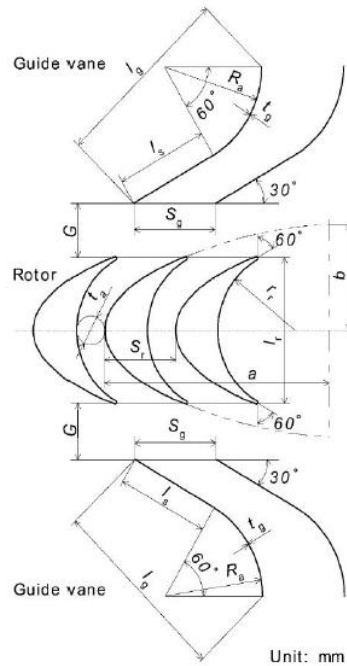
Fig.2: Rotor blade and guide vanes geometry

Therefore, the performance for the large diameter impulse turbines for actual wave energy power plants, running at higher Reynolds number can be predicted using the experimental data from model testing (Hammad, n.d; Setoguchi *et al*., 2004).

NUMERICAL PROCEDURE

In order to analyze the overall performance of the OWC device fitted with a full-scaled impulse turbine, iterations were carried out for various turbine rotational speeds between 60 and 900*rev/min*.

Considering the quasi-steady flow conditions, typical turbine characteristics arrived at from the uni-directional experimental data for the said turbine were used for this simulation as using such uni-directional flow data in the actual quasi-steady conditions has been validated by previous studies on the Wells turbine (Inoue *et al*., 1998) and a study on the impulse turbine (Setoguchi *et al.,* 2006). A simple geometry of the OWC (Setoguchi *et al.,* 2006) was considered for the simulation with a turbine duct area to air chamber area ratio, *m* = 0.0234 (see Fig.3). The techniques and performance parameters used by Inoue (1998) and Setoguchi *et al.* (2006) for the numerical simulation of 0:3m diameter Wells and impulse turbines under irregular flow conditions were adopted by Thakker *et al.* (2004). The latter analysis simulated the 0:6*m* impulse turbine using the existing equations with the damping term included so that it completed the general equation of motuion for column of water. It should be noted here that the calculation of OWC efficiency has been simplified to show how the damping applied by the turbine affects the overall efficiency of the device and is not reacting the true behaviour of an actual OWC. As

such, the simulation technique used does not take into account the effects due to the secondary damping which further consists of two components, namely, radiation damping due to waves by the column and loss damping due to energy losses in the system (Curran *et al*., 2000). This simplified technique was used to simulate irregular, unsteady flow conditions for the turbine, based on the sea wave data. The equations were solved using the standard numerical techniques using Runge-Kutta Fehlberg Method in Matlab (Thakker *et al.,* 2004).
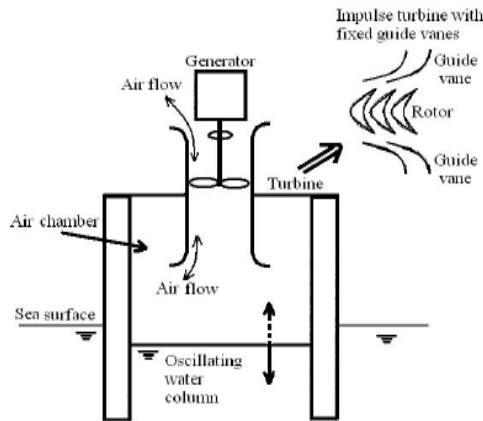
Fig.3: A schematic view of the OWC device used in the numerical simulation

Efficiency of OWC

The relationship between the incident wave height (H) and the wave height (h) in the air chamber is given by Setoguchi *et al.* (2006) as:

$$\frac{d}{dt}(\rho_s h A_C \frac{dh}{dt}) = \left\{ \rho_s g \left(H - h \right) - \Delta p \right\} A_C$$

(6)

This is an approximate equation of the motion of OWC because the equation of motion about OWC is generally expressed by using linear water wave theory (Chatry *et al*., 1999).

Eq. 6, which basically originates from Newton's second law of motion i.e. *F = m a*, was modified to include the damping applied by the turbine. The standard equation of motion for a mass-spring-damper system is given in the basic form as follows:

$$\frac{d}{dt}\left\{ m\dot{X} \right\} + C\left\{ \dot{X} \right\} + K\left\{ X \right\} = F(t)$$

(7)

where

$$F(t) = \left\{ \rho_s g \left(H - h \right) - \Delta p \right\} A_C \qquad \text{oscillating force on water column surface}$$

$$m = \rho_s h A_C = M_E \qquad \text{effective mass of water column}$$

$$C = B_A \qquad \text{damping}$$

$$K = \rho_s g A_C \qquad\qquad \text{the buoyancy of the column}$$

$$X = h \qquad\qquad \text{displacement of water surface.}$$

Considering the system analogous to the mechanical vibration system with single degree of freedom with damper, the equation of motion (Eq. 6) can be modified to include the damping applied by the turbine. This results in the following equation:

$$M_E = \frac{d^2 h}{dt_2} + B_A \frac{dh}{dt} + K\ h = F(t)$$

(8)

The damping applied on the OWC by the turbine, B_A, is given by:

$$B_A \frac{F(t)}{\upsilon_c} = \Delta p \frac{A_C}{\upsilon_c} = \Delta p \frac{A_C{}^2}{A_T\ \upsilon_a}$$

(9)

Given the flow coefficient,

$$\phi = \frac{\upsilon_a}{U_R}$$

(10)

which is the ratio of axial velocity to tangential blade velocity at mid-span (r_R), and

$$p^* = \frac{\Delta p}{\rho_a\ \omega^2 (2r_R)^2}$$

(11)

which is the definition of the pressure coefficient (Thakker & Fergal, 2004), substituting in B_A for p^* and φ gives:

$$B_A = 4\rho_a \frac{A_C{}^2}{A_T} U_R \left(\frac{p^*}{\phi} \right)$$

(12)

It has been reported that the optimum damping is a function of wave period, incident wave power, and that no single damping level will optimize the performance of the column in all seas (Curran *et al*., 1995). Substituting the values of M_E, B_A, K, X and $F(t)$ in Eq. 8 and simplifying, we will get:

$$\frac{d}{dt}(h\frac{dh}{dt}) + 4\rho_a \frac{A_C}{A_T} U_R \left(\frac{p^*}{\phi} \right) \frac{dh}{dt} + \frac{\Delta p}{\rho_s} + g(2h - H) = 0$$

(13)

The above equation was solved using Runge-Kutta Fehlberg algorithm Matlab. The turbine performance characteristics were taken from experimental data under steady conditions. Generally, it is believed that the characteristics of the irregular motion of the OWC are different from those of the incident waves due to the energy absorbing characteristics, losses due to

radiation, and other effects due to the random nature of the waves. As the main purpose of this simulation is to evaluate turbine performance under given irregular conditions, the method was simplified and only damping applied by the turbine was taken into account, while other factors were not taken in consideration here.

The conversion efficiency of OWC can be defined as the ratio of incident wave power and the power of OWC. It is important to note here that the efficiency of the air chamber is also dependent on the compressibility effects within the chamber (Thakker *et al*., 2003). However, as the objective of this analysis is to evaluate the performance of the turbine under real sea conditions, the efficiency of the air chamber in this case can therefore be obtained by the ratio of incident wave power and the power of OWC (Setoguchi *et al*., 2006). The incident wave power is defined as the power in watts delivered by each meter width of a wave (Duckers, 1996) and is given by:

$$W = \frac{\rho_s g^2 H^2 T}{32\pi}$$

(14)

Therefore, the incident wave power $\overline{W_i}$ and power of OWC $\overline{W_o}$ are defined as:

$$\overline{W_i} = \frac{\sum_{i=1}^{N} \frac{1}{32\pi} \rho_s g^2 H_i^2 T_i^2}{\sum_{i=1}^{N} T_i}$$

(15)

and

$$\overline{W_o} = \frac{\sum_{i=1}^{N} \frac{1}{32\pi} \rho_s g h_i^2 T_i^2}{\sum_{i=1}^{N} T_i}$$

(16)

Thus, the efficiency of air chamber can be defined as:

$$\eta_c = \frac{\overline{W_o}}{\overline{W_i}}$$

(17)

Efficiency of the Turbine

If compressibility effects are neglected, the air flow rate can be obtained by calculating the volume of water displaced above (or under) the mean water level (MWL) per unit time. Consequently, the axial flow velocity is directly proportional to a variation of the wave height *h*. Therefore, the non-dimensional axial flow velocity through the turbine v_a* is written as:

$$v_a* = \frac{d(h / H_s)}{d(t / \overline{T})} = \frac{dh*}{dt*}$$

(18)

The running characteristics of the turbine under irregular, unsteady flow conditions were calculated through numerical simulation. The steady flow characteristics of the turbine are assumed to be valid for computing performance under unsteady flow conditions. Such a quasi-steady analysis has been validated in some previous studies for both Wells turbine (Inoue *et al*., 1998) and impulse turbine (Setoguchi *et al*., 2006). The running characteristics are obtained by keeping rotational speed constant. In this case, the mean output $\overline{C_o}$ and input coefficient $\overline{C_i}$ can be defined respectively as:

$$\overline{C_o} = \frac{1}{t^*} \int_0^{t^*} C_T(\phi) \frac{\left(k\omega^*\right)^2 + \left(\upsilon_a^*\right)^2}{2} \sigma_r \frac{4(1-v)}{(1+v)} \overline{\omega}^* dt^*$$

(19)

$$\overline{C_i} = \frac{1}{t^*} \int_0^{t^*} C_A(\phi) \frac{\left(k\omega^*\right)^2 + \left(\upsilon_a^*\right)^2}{2k} \sigma_r \frac{4(1-v)}{(1+v)} \upsilon_a^* dt^*$$

(20)

It can be noted from Eq. 14 and 15 that the performance of the turbine can be calculated as a function of $k\omega^*$ and υ_a^*, when torque coefficient, $C_T(\varphi)$, input coefficient, $C_A(\varphi)$, solidity, σ_{rR}, hub to tip ratio, v and non-dimensional angular speed ω^* are specified.

The mean efficiency of the turbine can be defined as:

$$\eta_t = \frac{\overline{C_o}}{\overline{C_i}}$$

(21)

Therefore, the mean conversion efficiency for the OWC device at a given constant rotational speed under irregular, unsteady flow conditions can be calculated as follows:

$$\eta = \eta_t \bullet \eta_c$$

(22)

METHODOLOGY

In the above section, it was mentioned that the turbine performance under irregular conditions depends on a unique parameter $k\overline{\omega}^*$. This parameter includes the characteristic parameters of the irregular wave (H_s & $\overline{T}$), turbine speed (ω) and the dimensions of the turbine and air chamber (r_R & m). Therefore, once an optimum value of $k\overline{\omega}^*$ is determined by numerical simulation for a given test wave and dimensionless turbine characteristics, the combination of optimum design values (m, r_R and ω) can be obtained for a site where significant wave height, *Hs* an d mean time period $\overline{T}$ are known (Setoguchi *et al*., 2006).

The reciprocal $1/k\,\omega^*$ represents the flow coefficient for ordinary fluid machines. To calculate different $1/k\,\omega^*$ values, assuming quasi-steady flow conditions uni-directional steady flow experimental data at constant axial velocity was used to generate turbine performance data for different constant rotational speeds. The $C_T(\varphi$ and $C_A(\varphi)$ characteristics trends from experimental results were used to generate the turbine performance data for different constant rotational speeds. The turbine performance data were generated for different rotational speeds

between *900 rpm* to *60 rpm* in order to get a wide range of flow coefficient through the turbine.

After generating the performance data, the incident wave height was converted into wave height in the chamber for each constant rotational speed using Runge-Kuta-Fehlberg algorithm. Following this conversion, the wave height within the chamber was translated into the volume flow and non-dimensional axial velocity, v_a*, over the turbine. The variation of the damping (B_A) was calculated using instantaneous flow coefficient and pressure drop through the turbine. Subsequent calculations lead to the mean turbine output and input characteristics (Eq. 19 and Eq. 20, respectively). The mean efficiency of the turbine was achieved using Eq. 21. Similarly, the efficiency of the OWC was also calculated for each individual $1/k\ \omega*$ by using Eq. 15 and Eq. 16. Finally, the overall mean efficiency of the device was achieved by using Eq. 17 for each constant rotational speed.

Application To Typical Irish Sea State

The numerical simulation technique was used in this work to evaluate the energetic performance of an OWC device with reference to the sea state typical of an Irish location. The study was carried out using actual sea data based on the water surface elevation time history (Thakker *et al.*, 2008) measured during the years 2002-2003. It was referred as wave site-2, which has an overall mean time period, $\overline{T} = 9.2$s, and the mean significant height $H_s = 3.1$m. The wave site-2 data had been initially assessed for the reference year and 9 significant sea states were found (summarized in Table 2).

TABLE 2
The nine sea states for the climatic Irish wave site-2

Sea states	1	2	3	4	5	6	7	8	9
$H_s(m)$	0.8	2	2.9	3.8	4.6	5.2	6.6	7.4	8.9
$\overline{T}(s)$	7.4	8.8	9.7	10.3	11.7	12.0	12.7	13.2	13.5
$Z(\%)$	12.2	31.0	26.6	14.8	7.1	4.0	2.0	1.5	0.3

The wave frequency is defined in terms of its energetic period, $\overline{T}$. In Table 2, Z is the sea state frequency of occurrence in a year. Moreover, the input data used are shown as a diagrammatic view of both significant wave height (*m*) and wave period (*s*) versus time. In Fig.4 and Fig.5, the seasonal trend of wave data is shown for a typical winter and summer conditions, respectively, in terms of hourly distribution of H_s & $\overline{T}$. It is remarkable that the Irish sea conditions feature almost unchanged wave period distributions in terms of average values, but the winter significant height is usually higher. With respect to the reference year, the annual average level of the power released on the west coast of Ireland is about $35 \div 40$ *kw/m*.

As far as the input quantities (significant height and mean period) are concerned, they are given to the numerical technique Matlab programme with an hour time step during a year, from 1.00 am of September 1st to 12.00 pm of August 31st. In the following section, the January results are shown.
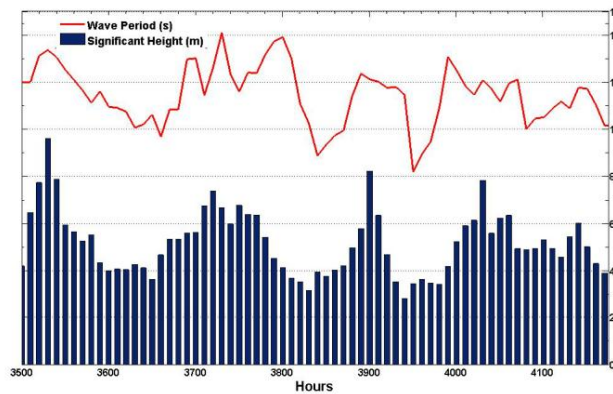
Fig.4: Wave input distributions in January 2002
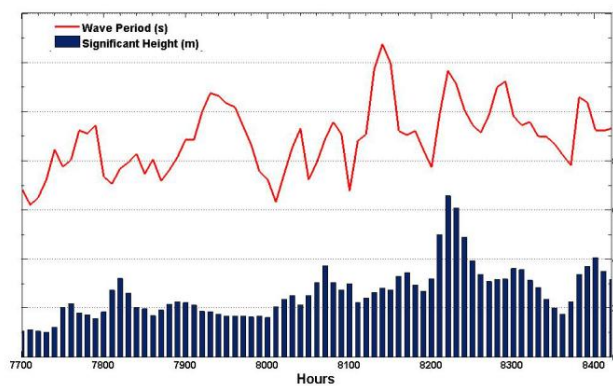
Fig.5: Wave input distributions in July 2002

Damping Applied by the Turbine

Fig.6 demonstrates the incident wave height (*H*) and wave height inside the chamber (*h*) plotted against time (*Hours*) for different turbine speeds (125, 200, 300, 400, 600, 700*rev/min*). It can be seen that there is a far greater variance in the scatter of the values of h at higher wave incidences. It can also be observed that as *H* decreases, this trend tends to die out and the values of h tend to converge towards a single value and closer to *H*. However, as *H* increases, it can be seen that the energy loss in converting to *h* increases dramatically. This conclusion is reached as the percentage of *h* retained after the conversion from H decreases accordingly as *H* increases.

Fig.6 also demonstrates the changing effect the turbine rotational speed has on the amount of damping applied by the turbine and hence the generated flow coefficient. It can be seen that as the turbine speed increases, the applied damping increases and the flow coefficient range of the OWC decreases.

Fig.7 shows the mean converted power incident wave to pneumatic, hourly integrated. The simulated system pneumatic power has a trend similar to the incoming wave conditions. It is worth noting that its values are irregular because of the large variability of the incident waves. This confirms that the output power from the OWC is higher for higher waves and vice

versa. This also resembles the typical behaviour of the turbine, as shown during uni-directional steady and unsteady flow conditions in terms of air axial velocity. Furthermore, it is noticed from Fig.7 that local maxima related to a particular speed exist at different levels of incident wave power. The OWC device converts more power when the turbine is running at 300rpm than any other speed when higher wave power is available. This shows that the damping applied by the turbine is optimum at 300rpm for such higher wave power. At a lower incident power, the OWC device converts more power at a higher turbine rotational speed. This is a clear indication that a higher level of damping does not indicate a lower performance of the OWC device; on the contrary, this could be optimum for a particular significant wave height.

In order to give more hints on the performance of the OWC device for different turbine speeds (200, 300, 400, 600*rev/min*), it is convenient to analyze the shaft torque output diagram. Fig.8 demonstrates the marked conversion discontinuities owing to the non-deterministic wave energy character. It can be seen that there is a far greater variance in the scatter of the values of turbine torque at the higher wave incident. It can also be observed that accordingly, as the incident power decreases, this trend tends to die out and the values of the turbine torque tend to converge towards a single value.
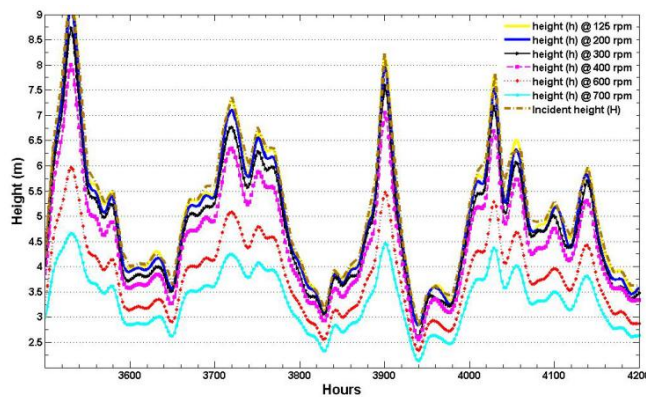
Fig.6: Incidence height (H) and height inside the chamber (h) versus time at different rotational speeds
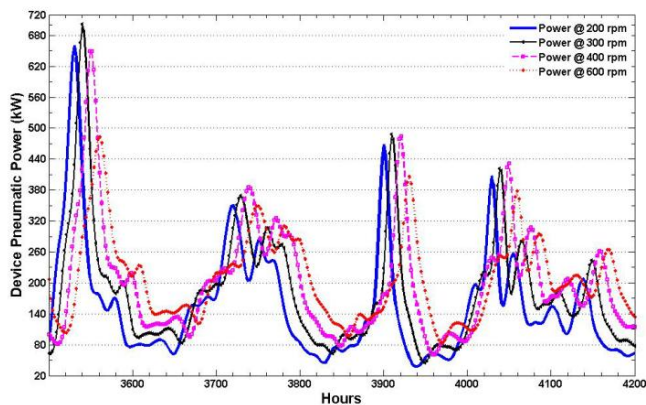
Fig.7: The OWC pneumatic power distribution in January
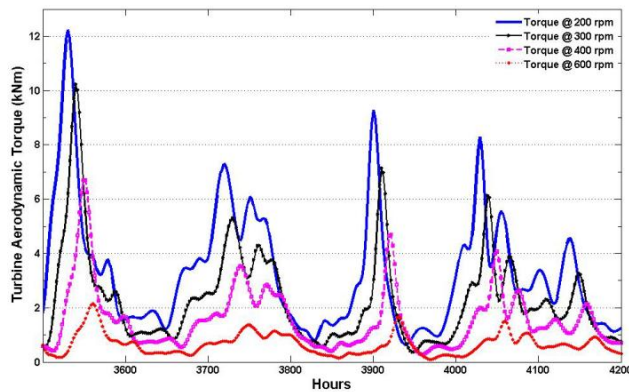
Fig.8: Turbine Torque distribution in January

However, as the incident power increases, it can be seen that the torque and hence the energy loss increases. Though the output torque at 200*rpm* is shown to be the highest, the shaft power is higher when the turbine is running at 300*rpm* because of the difference in the rotational speed. Furthermore, as shown previously, the converted pneumatic power available to the turbine is also higher.

Optimum Turbine Rotational Speed

One of the major parameters for the design of the impulse turbine for a wave power application is the rotational speed that the turbine is to be operated at. In Fig.9, different instantaneous efficiency profiles can be seen for the turbine over the range of input power when the turbine is operated at different rotational speeds. The higher the efficiency value (Fig.9) is about 46%, which corresponds to the optimum operating condition. This value of the peak conversion efficiency is in accordance with the available experimental data. In Fig.10, it can be seen that the corresponding shaft power produced at these rotational speeds. These last two figures are based essentially on the same information, but expressed in two different ways. Perhaps Fig.10 has a more immediate and intuitive meaning since it gives the output power directly.
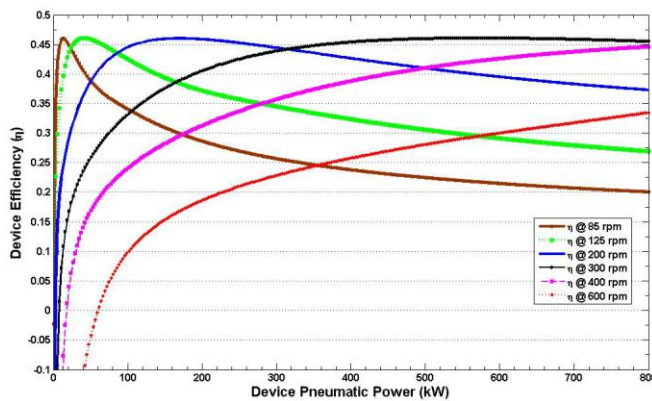
Fig.9: Device efficiency vs. available power
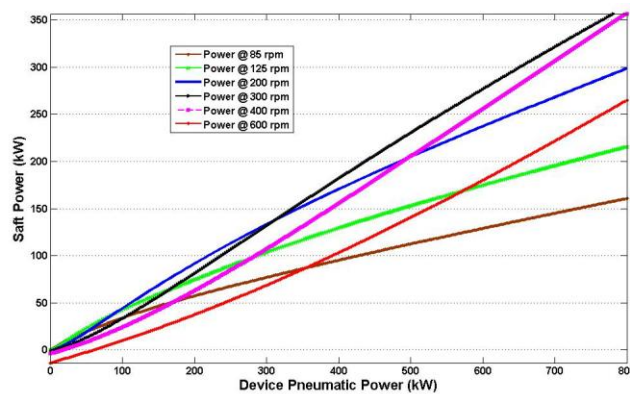
Fig.10: Shaft power vs. available power

The effect of efficiency peak occurring low in the input power range is apparent. Taking the efficiency curve corresponding to 85rpm shown in Fig.9 as a case in point, it can be seen that the efficiency characteristic of the turbine climbs rapidly to a peak at a low input power level. The impulse turbine with fixed guide vanes has a benign efficiency fall off characteristic after the peak efficiency point in comparison with the Wells turbine, which has a pronounced stall characteristic. There is no such characteristic in the impulse turbine with fixed guide vanes; this turbine still delivers useful amounts of power up to 800*kw* after it has reached its peak efficiency at a mere 20*kw*. However, this is clearly not the ideal manner in which to operate the turbine as can be seen from the corresponding curve in Fig.10.

Having the efficiency of the turbine peak low in the range of input power results in an inferior performance. In the case of the turbine being operated at 300*rpm*, Fig.10 shows that more power is delivered over a range of input power. In Fig.9, it is clear that the efficiency of the turbine peaks much closer to the mid range of input power. This results in the turbine converting a greater proportion of a larger input power, resulting in higher overall converted power. The integral OWC simulated performance is presented in Table 3, in terms of the monthly converted energy. These data are computed in time of the total power produced by the OWC device.

From the integration results, i.e. the total amount of energy converted by the OWC during a year is about 54 and 348*Mwh* when the turbine is running at 200*rpm* and 400*rpm*, respectively, with 40% of the total productivity from January and February. Critically, it was noticed that the productivity from July and August accounted for 20% of the total energy converted during the reference year, which is typical of the Irish climatic conditions. Finally, the mean turbine efficiency predictions, with and without damping along with the bi-directional unsteady flow experimental results, are shown in Fig.11. The predicted efficiency matches qualitatively the experimental efficiency results. From the curves in this plot, the effect of turbine damping can be observed, especially at higher values of $1/k\ \omega^*$. It can be noted here that in the flow conditions from this wave site, the magnitude of peak efficiency was comparable with that achieved under bi-directional unsteady flow conditions. However, the efficiency dropped significantly at higher flow coefficients as compared to that observed in the case without damping. The reason might be due to the fact that the pressure drop offered by the turbine in the region of higher flow

coefficient is comparatively very high and the curve is steeper than that of the experimental one. The peak efficiency dropped by a value of 2.5% from the experimental result of 43.5% (Rehil, 2007) at $1/k\,\omega^* = 1.2$, which was achieved under uni-directional unsteady flow conditions. It can be noted that the value of $1/k\,\omega^*$ corresponding to $300rpm$ at peak efficiency is different from the experimental value. This can be attributed to the fact that the turbine performance in the irregular wave conditions depends on the level of turbine damping, which in turns depends on the wave climate, especially the significant wave height. It can be said that turbine damping has a significant effect on the performance of turbine and also the overall performance of complete device.

TABLE 3
Monthly energy converted by the OWC device

	Energy (MWh)	
Month	200 rpm	400 rpm
Sept	1.35	11.38
October	2.42	32.74
November	1.74	6.27
December	1.59	13.52
January	11.72	70.06
February	8.55	76.16
March	1.37	14.71
April	4.78	33.02
May	3.44	22.16
June	2.64	22.34
July	4.18	10.31
August	10.40	35.98
Tot	54.23	348.72
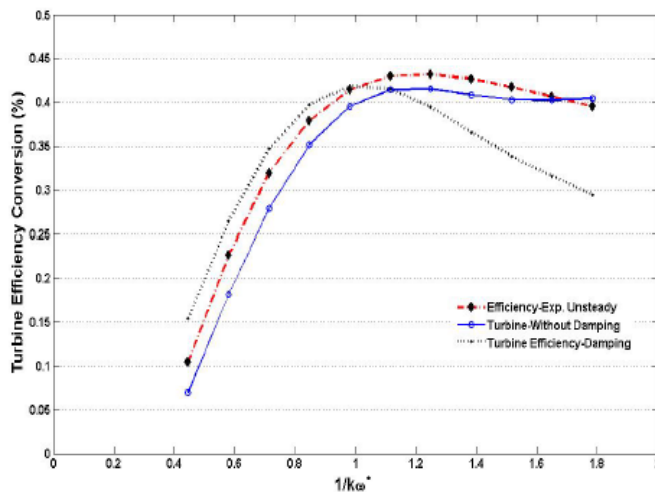
Fig.11: A comparison of turbine efficiency (with and without damping) and efficiency from the experiment

CONCLUSION

The performance of the turbine under irregular, unsteady flow conditions using real sea data shows that the damping applied by the turbine is a major factor affecting the energy conversion from raw sea waves. The results achieved using this numerical simulation technique show that it can be used as an indicative tool to predict turbine performance under irregular, unsteady flow conditions for specific wave conditions. The use of real sea data enhances the practical use of this numerical simulation for predicting performance of the turbine for an actual power plant for a given wave site. In order to exploit the maximum power from the waves, the turbine should be matched so as to give an appropriate level of damping for the prevailing wave conditions. The typical stable behaviour, associated with this type of turbine was observed under irregular, unsteady real sea conditions. No stall point was observed and therefore the turbine was able to perform consistently at varying wave conditions. This characteristic gives it an edge over other self-rectifying turbines used for wave energy extraction. Therefore, it can be said that this impulse turbine is capable of converting energy for a wide range of flow coefficient under irregular, unsteady flow conditions. The simplified technique was used to simulate irregular, unsteady flow conditions for the turbine based on sea wave data do not react the true behaviour of an actual OWC.

ACKNOWLEDGEMENTS

REFERENCES

de O. Falca~o, A. F. (2003). First-generation wave power plants: Current status and R & D requirements. *J. of O-Shore Mechanics and Arctic Engineering*, November, 2003.

Thakker, A., Khaleeq, H. B., & Ansari, A. R. (2001). Numerical Simulation of 0.6m Impulse Turbine for Wave Power Conversion under different Flow Conditions. Proceedings of the 11th (ISOPE 2001) International O_shore and Polar Engineering Conference, June 17-22, 2001, Stavanger, Norway, *1*, 634-637.

Thakker, A., Usmani, Z., & Dhanasekaran, T. S. (2004). Effects of turbine damping on performance of an impulse turbine for wave energy conversion under different sea conditions using numerical simulation techniques. *Renewable Energy, 29*, 2133-2151.

Thakker, A., & Fergal, H. (2004). Modeling and scaling of the impulse turbine for wave power applications. *J. of Renewable Energy, 29,* 305-317.

Setoguchi, T., Takao, M., & Kaneko, K. (2006). Current status of self rectifying air turbines for wave energy conversion. *J. of Energy Conversion and Management, 47*, 2382-2396.

Thakker, A., Sheahan, C., Frawley, P., & Khaleeq H.B. (2001). The concurrent engineering approach to the manufacture of impulse turbine blades using rapid prototyping. *The Rapid Prototyping Journal, 7*(3), 15. Proceedings ofthe RPA ofthe Society ofMechanical Engineers, USA.

Thakker, A., Jarvis, J., Buggy, M., & Sahed, A. (2008). A novel approach to materials selection strategy Case study: wave energy extraction impulse turbine blade. *J. of Material Design*.

Ryan J. (2005). *Experimental analysis of irregular unsteady ow on performance of impulse turbine for wave energy conversion*. MEng thesis, University of Limerick.

Hammad, B. K. (n.d.). *Design Analysis of the Impulse Turbine with Fixed Guide Vanes for Wave Energy Power Conversion*. Doctoral??

Setoguchi, T., Takao, M., Santhakuma, S., & Kaneko, K. (2004). Study of an Impulse Turbine for Wave Power Conversion: Effects of Reynolds Number and Hub-to-Tip Ratio on Performance. *J. O_shore Mech. Arct. Eng. 126*, 137-143.

Inoue, M., Kaneko, K., Setoguchi, T., & Saruwatari, T. (1998). Studies on the Wells Turbine for Wave Power Generation (Turbine characteristics and design parameters for irregular wave). *JSME International Journal, 31*, 676-682.

Curran, R., Denniss, T., & Boake, C. (2000). *Multidisciplinary design for performance: ocean wave energy conversion*. In Proceedings of the International O_shore and Polar Engineering Conference, p. 434-41. Seattle, Washington, USA, May 2000.

Chatry, G., Clement, A. H. & Sarmento, A. J. N. A. (1999). Simulation of a self-Adaptively Controlled OWC in a Nonlinear Wave Tank. Proceedings of the 9th (ISOPE-1999) International O_shore and Polar Engineering Conference, Brest, 3, 290-296.

Curran, R., Raghunathan, R. S., Stewart, T. P., & Whittaker, T. J. T. (1995). Matching a Wells Turbine to the Islay oscillating water column wave power converter. In Proceedings of the International Conference on O_shore Mechanics and Arctic Engineering 1995, p. 14754 (Copenhagen, Denmark, June 1822).

Thakker, A., Dhanasekaran, T. S., Takao, M. & Setoguchi, T. (2003). Effects of Compressibility on the Performance of a Wave- Energy Conversion Device with an Impulse Turbine Using a Numerical Simulation Technique. *International Journal of Rotating Machinery, 9*, 443-450.

Duckers, L. (1996). Chapter 8 - Wave Energy. In G. Boyle (Ed.), *Renewable Energy - Power for a Sustainable Future* (pp. 315 – 352). Oxford University Press.

Rehil O.A. (2007). *Experimental analysis of sel-rectifying turbines operating uni-directional steady flow and bi-directional unsteady flow for wave energy conversion.* Doctoral Thesis, UL (WERT).

APPENDICES

Symbol	Description
A_C	area of chamber
A_T	area of turbine
b	blade height
B_A	applied damping
C_A	input coefficient
C_T	torque coefficient
Δp	pressure drop
G	gap between rotor and guide vane
H	incident wave height
h	wave height in the chamber
l_g	chord length of guide vane
H_s	significant incident wave height
$\overline{T}$	mean wave period
l_r	chord length of rotor blade
m	A_T/A_C
P^*	pressure coefficient
Re	Reynolds number
r_R	mid span radius
S_g	guide vane pitch
S_r	rotor blade pitch
T	torque
U_R	circumferential velocity at r_R
v_a	axial flow velocity
v_c	air velocity at water column surface
z	number of rotor blades
ϕ	flow coefficient
γ	rotor blade inlet angle
η	turbine efficiency under steady flow
ν	hub to tip ratio
θ	setting angle of fixed guide vane
ρ_a	density of air
ρ_s	density of sea water
ω	angular velocity of turbine rotor
$\omega^* = \omega\overline{T}$	non-dimensional angular velocity
$k = \dfrac{m\, r_R}{H_{1/3}}$	
$t^* = \dfrac{t}{T}$	non-dimensional time
$\phi = \dfrac{v_a^*}{K\omega^*}$	flow coefficient
ν	hub to tip ratio
σ_{rR}	solidity of rotor at r_R
$v_a^* = \dfrac{m\overline{T}v_a}{H_s}$	
$k\omega^* = \dfrac{\omega m r_R \overline{T}}{H_s}$	
$\overline{\omega^*} = \omega\overline{T}$	